Mon. Not. R. Astron. Soc. **000**, 000–000 (0000) Printed 17 February 2005 (MN LATEX style file v2.2)

A non-main-sequence secondary in SY Cancri

Robert Connon Smith⋆, Otto Mehes, Dave Vande Putte, Nigel A. Hawkins
Astronomy Centre, Department of Physics and Astronomy, University of Sussex, Falmer, Brighton BN1 9QH, UK

Accepted 200 . Received 200 ; in original form 200

ABSTRACT
Simultaneous spectroscopic and photometric observations of the Z Cam type dwarf nova SY Cancri were used to obtain absolute flux calibrations. A comparison of the photometric calibration with a wide slit spectrophotometric calibration showed that either method is equally satisfactory. A radial velocity study of the secondary star, made using the far red Na I doublet, yielded a semi-amplitude of $K_2 = 127 \pm 23\,\mathrm{km\,s^{-1}}$. Taking the published value of $86 \pm 9\,\mathrm{km\,s^{-1}}$ for K_1 gives a mass ratio $q = M_2/M_1 = 0.68 \pm 0.14$; this is very different from the value of 1.13 ± 0.35 quoted in the literature. Using the new lower mass ratio, and constraining the mass of the white dwarf to be within reasonable limits, then leads to a mass for the secondary star that is substantially less than would be expected for its orbital period if it satisfied a main-sequence mass-radius relationship. We find a spectral type of M0 that is consistent with that expected for a main-sequence star of the low mass we have found. However, in order to fill its Roche lobe, the secondary must be significantly larger than a main sequence star of that mass and spectral type. The secondary is definitely not a normal main-sequence star.

Key words: stars: dwarf novae – novae, cataclysmic variables – stars: individual: SY Cnc

1 INTRODUCTION

The cataclysmic variable (CV) SY Cancri is listed in the Ritter & Kolb (2003) catalogue of CVs as a Z Cam type dwarf nova with a period of 0.380 ± 0.001 days (9.13 ± 0.024 hours). In common with most Z Cam stars (Warner 1995, p.165), there are no eclipses, the published inclination being $26° \pm 6°$ (Shafter 1983). An intriguing result is the mass ratio, which is given by Shafter (1983) as $M_2/M_1 = 1.13 \pm 0.35$. Despite the large uncertainty, this suggests that the secondary star could be the more massive of the pair. If true, this would be rather surprising, since the canonical picture of mass transfer in CVs assumes that the secondary star is less massive than the white dwarf. Mass transfer can then proceed on a slow timescale determined by the rate of angular momentum loss from the system (e.g. A. King 1988). If the secondary is the more massive component, it should be transferring mass on a *dynamical* timescale (A. King 1988). There is no evidence for that in SY Cnc. Since we made our observations, more detailed calculations by Politano (1996) have shown that the situation is more complicated than this, and estimates from his Figure 2 show that the system would be stable with this mass ratio if the mass of the secondary in solar masses were in the range 0.75 to 1.30. None the less, the Shafter mass ratio is unusually large and, as we shall see, stability criteria do play a role in determining the parameters of the system.

Shafter's mass ratio estimate is based on detection of emission lines only, together with an empirical calibration (Shafter 1983) of a relationship between the mass ratio and the width of the Hα *emission* line, interpreted as a rotation velocity in the disc. It seemed more plausible that this relationship is violated in SY Cnc than that the secondary is really the more massive component, but only a direct detection of the absorption line spectrum of the secondary star could verify that. We therefore decided to try to make a direct measurement of K_2 to check the mass ratio and test the assumption made by Shafter. We planned to use the Na I doublet near 8200 Å, which had been successfully used to measure radial velocities for other secondary components (Friend et al. 1990a, b).

The long period suggests that the secondary should be relatively massive ($\sim 1\,\mathrm{M}_\odot$) if it is on the main sequence and fills its Roche lobe, as is commonly the case for CV secondaries (Smith & Dhillon 1998). This mass corresponds to an early to mid G type star (which is consistent with a recent spectral type estimate of G2 from IR spectra – Harrison et al. 2004). However, Patterson (1981) reported a late G type spectrum, while Szkody (1981) said that a secondary with an effective temperature of $\simeq 4500$K was needed to fit the UV, optical and IR spectra, which suggested an early K type spectrum. These discrepancies already suggested that

⋆ E-mail: rcs@sussex.ac.uk

Night No.	Date 1989 April	UT Start Time	Exposure Time (secs)	HJD mid-exposure (-2447600.0)	Skyshift ($km\,s^{-1}$)	Heliocentric Correction ($km\,s^{-1}$)	Notes
1	13/14	20:50	1024	30.3762728	0.00000	0.03	R831R grating.
		21:12	1024	30.3915678	0.00000	0.06	
3	15/16	22:19	1024	32.4379346	0.00000	0.19	
		22:58	1024	32.4651007	0.00000	0.24	
		23:17	1024	32.4779764	3.98127	0.26	
		23:37	1024	32.4913055	0.00000	0.28	
		23:58	512	32.5039073	0.00000	0.31	Wide slit.
		00:11	512	32.5128255	0.61694	0.32	Wide slit.
4	16/17	21:27	1024	33.4014396	0.00000	0.11	R400R grating from here on.
5	17/18	20:27	1024	34.3591914	0.00000	0.01	
		20:49	1024	34.3752031	0.00000	0.05	
		21:09	1024	34.3881816	-1.98700	0.08	
			1024	34.4005943	-3.11917	0.11	
			1024	34.4130141	-8.13713	0.14	
			1024	34.4254154	34.13813	0.17	
			1024	34.4378249	0.00000	0.20	
		22:41	1024	34.4528655	0.00000	0.23	
			1024	34.4652682	3.15828	0.25	
			1024	34.4776773	0.76570	0.27	
		23:40	1024	34.4938585	0.41650	0.30	Wide slit.
		00:03	1024	34.5096814	0.00000	0.32	Wide slit.
6	18/19	20:46	1024	35.3729502	0.00000	0.05	
			1024	35.3853784	0.92120	0.08	
			1024	35.3978143	6.25017	0.11	
			1024	35.4102357	-9.07470	0.14	
			1024	35.4226507	-3.83577	0.17	
			1024	35.4350579	0.00000	0.19	
		22:44	1024	35.4547941	0.00000	0.23	
			1024	35.4672223	3.25285	0.25	
			1024	35.4796619	9.16655	0.28	
			1024	35.4921105	-0.76024	0.30	
			1024	35.5045500	0.00000	0.31	
7	19/20	21:23	1024	36.3985788	0.00000	0.12	
			1024	36.4110005	2.40349	0.15	
			1024	36.4234270	5.71727	0.17	
			1024	36.4358591	3.62479	0.20	
			1024	36.4482748	6.37748	0.23	
		22:55	1024	36.4624989	-1.04306	0.26	
			1024	36.4749092	-1.53231	0.28	
			1024	36.4873283	-1.17674	0.30	
			1024	36.4997447	0.00000	0.32	
		00:09	1024	36.5140711	0.00000	0.33	

Table 1. Journal of spectroscopic observations of SY Cnc. Most of the observations were taken at the lower resolution, to obtain wider wavelength coverage. No observations of SY Cnc were taken on night 2 (April 14/15)

the secondary is not quite normal. The rather early spectral type meant that we would not expect the Na I doublet to be easily detectable, but Friend found a possible detection in his work (see Friend et al 1988). The system was in outburst at that time, making the detection harder, so we hoped to be able to obtain a good radial velocity curve if we found the system in quiescence. In practice, the system appeared to be on decline from outburst, but the Na I doublet was still both detectable and measurable.

2 OBSERVATIONS AND DATA REDUCTION

2.1 Observations

2.1.1 Spectroscopy

We obtained 42 spectra of SY Cnc spread over six nights in 1989 April, as part of a more extensive observing programme using the Intermediate Dispersion Spectrograph on the Isaac Newton Telescope at the Roque de los Muchachos Observatory on the island of La Palma. We used the 235 mm camera and a GEC CCD. Of these spectra, 8 were taken at a dispersion of 1.121 Å/pixel and the remaining 34 at 2.304 Å/pixel, including several wide slit spectra. The corresponding wavelength ranges were 7662 – 8308 Å and 6951 – 8280 Å. Table 1 gives a full journal of the observa-

System	Date	Spectral Type	RV	Helio. Corr.	Notes
Gl 673	19/20	K7V	95.66	0.10	2.304 Å/pixel
Gl 488	18/19	M0.5e	27.69	0.08	
Gl 205	17/18	M1	8.52	0.31	
Gl 393	16/17	M2	8.36	0.29	
	17/18		8.36	0.28	
Gl 701	17/18	M2	32.47	0.07	
Gl 752A	16/17	M3	35.82	-0.08	
Gl 654	15/16	M3.5	34.60	0.15	
Gl 555	19/20	M4	28.62	-0.12	
Gl 285	16/17	M4.5	26.59	0.11	
Gl 699	15/16	M5	-110.86	0.07	
Gl 473	18/19	M5.5e	15.50	0.10	

Table 2. Red dwarf radial velocity standards observed at low resolution on the different nights in 1989 April.

Night No.	Date 1989 April	Time UT	Number of Exposures	Exposure Time (secs)	Comments
1	13/14	21:02–21:40	6	various	UBVRIZ colours only.
4	16/17	21:13–21:16	1	128	I band.
5	17/18	20:52–20:59	2	64	I
		20:59–21:29	30	32	I
		21:29–21:37	4	various	UBVR colours.
		21:52–00:34	105	32	I band. Brief gap for standard.
6	18/19	21:21–00:15	167	32	I
		00:28–00:33	4	various	UBVR colours.
7	19/20	20:39–21:45	62	32	I
		21:45–21:52	4	various	UBVR colours.
		22:12–22:53	32	32	I
		23:15–00:45	71	32	I band. Brief gap for standard.

Table 3. Journal of all photometric observations of SY Cancri. The table does not include several points which were unusable for various reasons. The most common reasons were the frame being saturated, the telescope moving during an exposure, or software problems causing frames to be either lost or corrupted. The single I-band exposures taken on nights 1 and 4 were not used.

tions. A copper-argon/copper-neon arc spectrum was taken at one- or two-hourly intervals during the observations, to provide wavelength calibration and to correct for instrumental flexure and instability. Spectra of the spectrophotometric standards HD 84937, Feige 34, BD+26°2606 (Oke & Gunn 1983) and BD+25°3941 were also taken in order to remove the telluric absorption features and correct for the instrumental wavelength response. Eleven single red dwarfs in the spectral type range K7 to M5.5 were observed at low resolution to allow spectral type calibration. The details are given in Table 2.

2.1.2 Photometry

We also observed SY Cnc photometrically on 4 nights, using a GEC CCD on the Jacobus Kapteyn Telescope. On the first night only colours were observed, while a long time series of I-band data was taken on each of the other 3 nights. Table 3 gives a full journal of the observations. We achieved significant overlap between the spectroscopic and photometric sets of observations on 3 nights (nights 5, 6 and 7), allowing us to undertake flux calibration both by using the simultaneous photometry and by using the wide slit spectra and the standard stars. This enabled an interesting comparison of the two methods of absolute flux calibration and also allowed us to check whether the slit losses were "grey" or wavelength dependent.

2.1.3 Ephemeris

The ephemeris used for all the light and radial velocity curves was the one given by Vande Putte et al (2003):

$$\mathrm{HJD} = 2447630.6195678 + 0.380\,E\ .$$

The period is not very precisely known, but the precision cannot be improved by our relatively short data run.

2.2 Data reduction

2.2.1 Spectroscopy

After the usual debiassing and flatfielding, the spectra were reduced using the method of optimal extraction (Horne 1986). For the wavelength calibration, sky emission lines were used to check the interpolation of the calibration between arc exposures. The continuum extinction was removed by using the tabulated average values for the extinction per unit airmass on La Palma (D. King 1988). The atmospheric

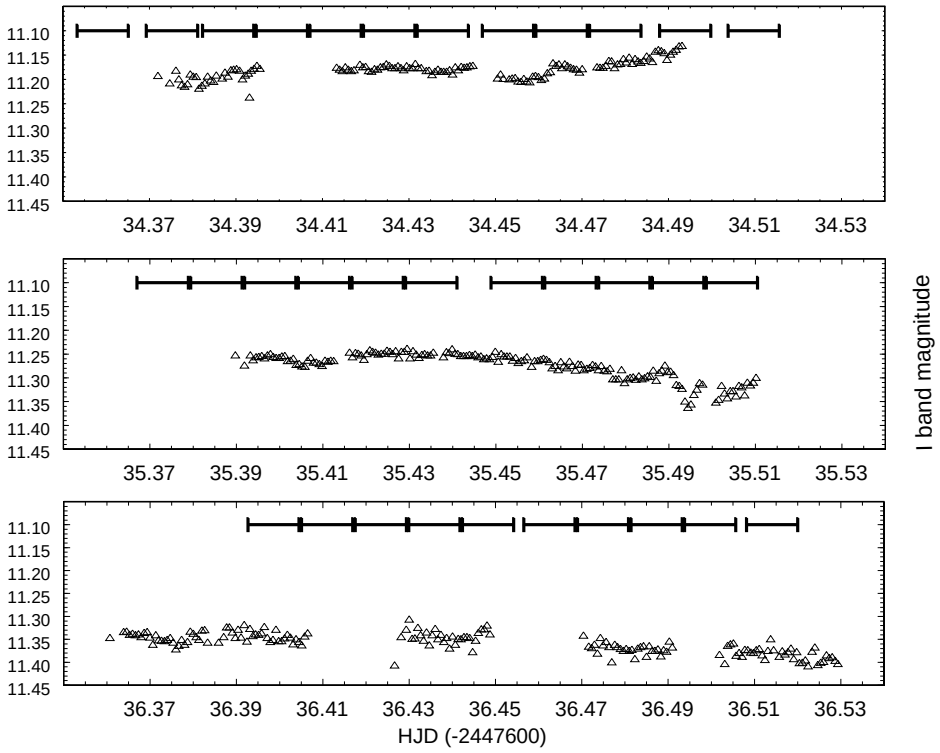

Figure 1. The 3 nights of simultaneous photometric and spectroscopic data for SY Cnc (top: night 5; middle: night 6; bottom: night 7). The triangles are the I band photometry points and the bars show the exposure durations of the spectra.

absorption was removed by using the standard stars to create a template showing the fractional absorption in each wavelength bin. For each spectrum, the standard star spectrum taken nearest in time to the object spectrum was used; Feige 34 was used for the wide slit spectra. Finally, the spectra were flux calibrated using the standard star Feige 34. This provided relative fluxes, but not absolute flux calibration, because of slit losses. The correction for slit losses is discussed in the next section.

2.2.2 Photometry

The CCD frames were first debiassed and flat-fielded and then the raw magnitudes were obtained for SY Cnc and for the comparison and standard stars by using aperture photometry. The wavelength-dependent extinction was taken from the tables of Argyle et al. (1988) for La Palma; the correction for the I band is 0.0174 mag. The wavelength independent dust component was removed by taking the values of *total* V-band extinction measured every night at the Carlsberg Automatic Meridian Circle and subtracting the tabulated wavelength-dependent component for the V band. Photometric standard stars chosen from the list of Argyle et al. (1988) were used to put the raw magnitudes on the absolute scale defined by Cousins.

Fig. 1 shows the I-band photometry data for SY Cnc for the 3 nights, together with the exposure times of the spectra. The photometry data have been corrected for all atmospheric effects, as described above, and show a very clear decrease in brightness over the 3 nights. Table 4 gives a summary of the magnitudes in all the observed wavebands during the run. Ritter & Kolb (2003) quote the V band magnitude to be about 10.9 in outburst, 12.2 in standstill and 13.5–14.5 in minimum, so the system appears to have been on the decline from an outburst at the time of our observations. None the less, as we shall see below, we were able to detect the secondary star.

Night of run	Cousins magnitude in band: U	B	V	R	I
1	10.835	11.533	11.340	11.325	11.027
5	10.516	11.432	11.448	11.341	∼11.17
6	10.746	11.590	11.543	11.441	∼11.3
7	10.800	11.667	11.614	11.491	∼11.35

Table 4. Multi-colour photometry of SY Cnc. Colours were measured at most once per night, all long series of observations being made in the I band. Typical exposure times were 32 seconds for the I and U bands and 16 seconds in the other bands (where the instrument has a better response). Errors were typically ±0.03 magnitudes in all bands.

3 SIMULTANEOUS PHOTOMETRY OR SPECTROPHOTOMETRY?

Unlike the photometric data, the spectroscopic data are rather difficult to put on an *absolute* flux scale. The main reason for this is the presence of *slit losses*, caused by some of the light of the star failing to pass through the slit. The amount of light which does pass through the slit depends on several factors:

(i) Slit Width — We need to use a narrow slit to ensure that we get the maximum spectral resolution possible with the instrumental setup being used, but this means that some light is likely to miss the slit. Assuming other factors to be constant, this will introduce a systematic error in the mean level of the spectra.
(ii) Positioning — If the object is not centred correctly on the slit, then light will be lost. Any slight drift in the pointing etc. will move the position giving rise to losses differing from frame to frame.
(iii) Seeing — In poor observing conditions, the light from the object is spread out more, and so a wider slit is needed to gather all the available photons. A further complication here is the possibility that the size of the seeing disc may vary with wavelength, so that rather than just producing variations in mean level, the shape of the spectrum may be distorted.

Fortunately, there are two methods of correcting for these losses, using simultaneous observations either of the same object photometrically or of a nearby non-variable comparison star spectroscopically.

Simultaneous Photometry. This method requires the use of a second telescope to obtain the photometric data simultaneously with the spectroscopic observations, but is slightly easier to perform than the comparison star method. For every spectrum taken of the object, one or more simultaneous photometry points in the waveband which matches the spectrum limits most closely are needed. The average magnitude of these is converted to the relevant flux density units and the average level of the spectrum is corrected to equal this level. The spectra were all centred in the wavelength range 7600–7900 Å, so the I-band data were appropriate for the calibration.
The first stage in the process was to find the average magnitude of all the photometry points which overlap with each spectroscopic exposure. The Cousins I magnitude was then converted to a flux density in mJy using the following relation (based on data from Bessell 1979):

$$\log_{10} f_\lambda = \left(\frac{I - 16.016}{-2.5}\right).$$

The corresponding error relation is:

$$\frac{\Delta f_\lambda}{f_\lambda} = -0.921 \Delta I.$$

Our typical error of ± 0.03 magnitudes thus gave an error of approximately ± 3 per cent in flux density. The major problem with this method is that although the mean level of the spectra is corrected, it is not possible to correct for any wavelength-dependent losses that would distort the spectral shape.

Comparison Star Spectra. This method requires that a second (non-variable) star is positioned on the slit together with the object. It also requires that at least one spectrum is taken of the two stars and of a flux standard, in photometric conditions, with a very wide slit to ensure that slit losses can be accurately removed. Ideally, the wide slit object spectra should be taken immediately before or after the wide slit standard star spectrum so that atmospheric variations between the two exposures are kept to a minimum. This wide slit standard spectrum is then used to flux calibrate the wide slit object and comparison star spectra. The standard star used here is Feige 34, for which the spectrophotometric data were obtained by Oke (1990). The wide slit spectra are assumed to show no slit losses and hence to provide an accurate continuum level across the whole spectral range on an absolute scale. Note that since a wide slit was used, the spectrum will not show line features very accurately. Polynomials were now fitted to the continuum of both the wide and narrow slit comparison star spectra. Each narrow slit object spectrum was corrected for slit losses by multiplying it by the ratio of the comparison star wide slit continuum fit to the appropriate comparison star narrow slit continuum fit. Thereafter, the resulting spectra were multiplied by the ratio of a polynomial fit to the tabulated spectrophotometric standard spectrum to a polynomial fit to our observed wide slit standard spectrum. Both adjustments are, of course, wavelength-dependent.
There is a problem with this method in that the need to place a comparison star on the slit means that in general the observations are made with the slit not at the parallactic angle (i.e. not vertical). This can be important since the atmosphere (especially at large airmasses) acts as a weak prism and spreads the incoming starlight slightly in the vertical direction. Having the slit vertical should ensure that all the light spread in this way enters the slit. With the slit not vertical, in order to obtain comparison star spectra, some of the light may miss the slit. This problem is compounded if the wavelength response of the TV guider differs from that of the detector as the telescope may appear to be perfectly aligned but actually be missing most of the light at the desired wavelengths. In addition, careful alignment of the slit is necessary to ensure that both stellar images are central on it, otherwise slight drift in the telescope positioning could lead to the recorded flux from the stars varying in relation to each other as one may drift off the slit while the other moves further onto it. The use of wide slit spectra should compensate for any errors due to the atmospheric prism effect but not necessarily for bad alignment of the slit.

Either of these methods should absolutely calibrate the spectroscopic data, though only the latter will correct for any wavelength dependence in the slit losses. Usually, one or the other of these methods is used, but it was pointed out to the authors (Dhillon 1990 and private communication) that there seems to have been no comparison between the two methods. As shown in Fig. 1, we have I band photometry simultaneous with 29 of the lower dispersion spectra. All of these object spectra also had comparison star spectra on the chip, and two of the spectra were taken with a wide slit, giving us all the data necessary to compare the two methods of absolute calibration.

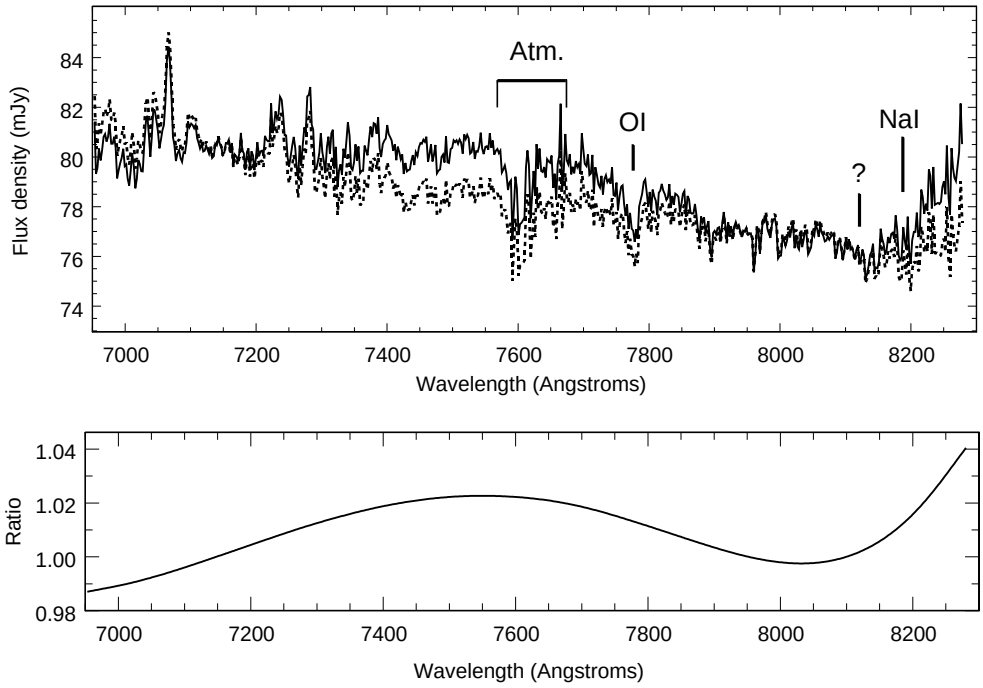

Figure 2. The top panel shows the average SY Cnc spectrum flux-calibrated using comparison star spectra (dotted line) and simultaneous photometry (solid line). A few spectral features and the atmospheric A band are marked, including the unidentified feature (?) mentioned in section 4. The bottom panel shows the ratio of the two spectra.

All 29 object spectra were flux calibrated using both methods described above, and then averaged. Fig. 2 shows the two average spectra and a comparison between them. The comparison is computed from the average of 29 spectra, each of which individually has an uncertainty of about 3 per cent, so we expect a scatter of about $(3/\sqrt{29})$ per cent or $\sim$ 0.5 per cent in the average and about 0.7 per cent $(0.5\times\sqrt{2})$ in the ratio. The comparison shows a slight systematic difference of about 2 per cent between the two methods, but the ratio shows only small ($\sim$ 1 per cent) variations from a straight line, which indicates that the slit losses are almost wavelength independent. The curve appears to be very smooth, but this is expected since the spectrophotometry process uses polynomials fitted to the spectra to correct for slit losses. The origin of the 2 per cent difference between the spectra is unknown, but is likely to stem from a small error in the zero point calibration of the photometry. We also note that the I band photometry is centred at a wavelength of around 9000 Å, whereas the spectra are centred around 7600 Å; this might also lead to a small zero point difference. The zero point error can be estimated from the equation above to be about 0.02 magnitudes.

This result means that the two calibration techniques are essentially identical (at least over this wavelength range) and so either may be used without introducing unnecessary errors. Thus it is possible to choose whichever method is most convenient in a given observing situation. The factors to be considered are:

(i) Use of resources. The simultaneous photometry method normally requires a second telescope. This will usually be difficult or impossible to achieve, making the comparison star spectrophotometry method the preferred choice in most situations. What we have demonstrated here is that it is no less accurate.

(ii) Wavelength dependent slit losses. The above analysis shows the slit losses to be 'grey' over this wavelength range, but this may not necessarily be true over other (particularly much wider) ranges and then spectrophotometry is essential.

(iii) Differential refraction. Because the use of a comparison star does not allow the slit to be used at the parallactic angle, there is always a residual effect of differential refraction in spectrophotometric calibration, and it is important to work as close to the zenith as possible.

(iv) Availability of a comparison star. The other big disadvantage of the spectrophotometry method is that there must be a non-variable comparison star near enough to the object to fit on the slit, and this may not always be true. In such cases simultaneous photometry must be used for absolute calibration. Our results suggest that, at least for small wavelength ranges, this may be done without distorting the resultant spectra.

(v) For echelle spectra, the orders are generally too closely spaced on the CCD to allow the spectrum of a comparison star to be included in the same exposure. Simultaneous photometry is then essential, but in practice is hard to obtain if one wishes to use 8-m class telescopes: for example, there is

no readily available photometric telescope available on the same site as the VLT.

4 RADIAL VELOCITY STUDY

4.1 Sodium doublet velocities

Given Shafter's (1983) measurements of $86 \pm 9\,\mathrm{km\,s^{-1}}$ for K_1 and 1.13 ± 0.35 for the mass ratio, q, we would expect the secondary to be a late G or early K type star, and to give a radial velocity curve having a K_2 of $76 \pm 25\,\mathrm{km\,s^{-1}}$. Our earliest red dwarf cross correlation template was only K7, as the majority of the systems we were looking at have much shorter periods than SY Cnc and so the later templates were more generally useful. There was thus a danger that we would be unable to obtain a good radial velocity curve due to template mismatch, which has been indicated to be a significant source of error by Tonry & Davis (1979). The cross-correlation was run using the full range of templates available (K7 to M5.5) to try to minimise errors due to mismatch; it turned out that the best match was the K7 template, leaving some doubt at this stage about whether an earlier spectral type might provide a better fit (but see further discussion below, in the context of our skew mapping).

All the initial cross correlation results were found to be very noisy, with a blueshift of about $1200\,\mathrm{km\,s^{-1}}$ being indicated on several frames. All the frames were examined by eye, and it was found that there was an absorption feature centred at about 8150 Å, which could not be identified with any K or M dwarf feature in the Turnshek et al. (1985) spectral atlas. This feature showed most strongly in those frames giving the very high blueshift, with a strength roughly equalling that of the nearby 8190Å sodium doublet (this unidentified feature is marked on Fig. 2 with a question mark). In the late K and early M dwarf spectra being used for templates, the 8190Å Na I doublet is by far the strongest feature in the region used for the cross correlations. The unidentified feature is of roughly the same width as the Na I doublet, and at roughly the right wavelength to give the $1200\,\mathrm{km\,s^{-1}}$ blueshift measured if it is picked up by the cross correlation routine in preference to the doublet. This feature was assumed to be the source of the noise and was masked out in later cross correlation attempts. Further discussion of this feature is given in Section 4.2.

After masking out the unidentified feature, the cross correlation procedure was repeated, again using all the available templates, and was now found to give much less noisy results. Any template spectrum of spectral type K7 to M1 gave fairly good results in terms of noise level, though five very noisy spectra had to be excluded from the process as they gave wildly varying shifts depending on the template used. The template giving least noise was Gliese 673 (K7V), and Table 5 lists the cross-correlation results from using this template. The corresponding value of K_2 was found to be $168 \pm 15\,\mathrm{km\,s^{-1}}$. The tests given by Bassett (1978) were used to test whether there was any significant ellipticity in the orbit. None was found, and Fig. 3 shows the circular orbit fit corresponding to the parameters in Table 6. When the spectra are shifted and averaged using these parameters the Na I doublet is significantly enhanced, and the value of K_2 was

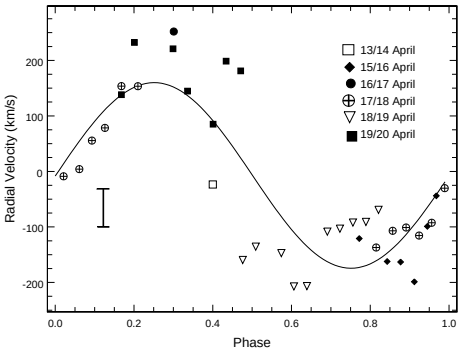

Figure 3. Circular orbit fit to SY Cancri data. The points are coded to show the night they were taken on and the bar in the bottom left indicates the size of the RMS deviation from the fit.

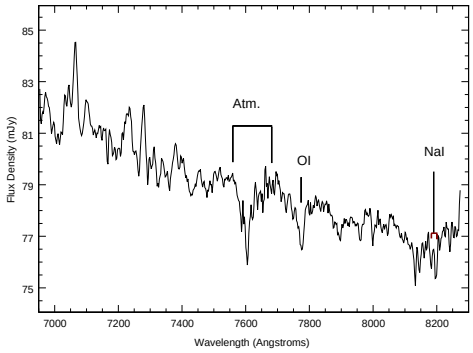

Figure 4. Mean spectrum of SY Cancri. The individual spectra which make this up have been shifted to correct for the motion of the secondary star before adding. A few spectral features and the atmospheric A band are identified.

used in a preliminary account of this work (Smith, Hawkins & Mehes 1999), which reported a mass ratio of 0.51 ± 0.07.

However, this radial velocity curve is still very noisy, as shown by the very large dispersion, and the large effect of removing the unidentified feature makes the result questionable. We therefore decided to adopt instead the technique of skew mapping (Smith et al. 1993a) which is designed to make optimum use of all the spectra. Essentially, the technique consists of calculating all the cross-correlation functions, as above, but then instead of using the individual velocity shifts the next step is to use back-projection on the cross-correlation functions to produce a map in velocity space. Each point in the map is the line integral over all the cross-correlation functions following the sine curve with the particular amplitude and phase at that point in the map. When calculating the cross-correlation functions, we masked out all the spectral region shortward of 7800 Å, to avoid the OI absorption feature and the strong telluric A band around 7600 Å. We also had an optional mask for the region 8125 to 8175 Å, to test the effect of the unidentified feature. The skew map was unaffected by whether or not we masked out the region containing the unidentified feature, showing the ability of skew mapping to screen out outliers.

HJD	RV (kms^{-1})	HJD	RV (kms^{-1})	HJD	RV (kms^{-1})
30.3762728	***	34.4254154	-30.08	35.4672223	-103.21
30.3915678	-23.54	34.4378249	-8.94	35.4796619	-92.07
32.4379346	-120.87	34.4528655	4.14	35.4921105	-90.94
32.4651007	-162.32	34.4652682	55.63	35.5045500	-69.19
32.4779764	-163.18	34.4776773	78.46	36.3985788	138.29
32.4913055	-198.92	34.4938585	153.61	36.4110005	232.29
32.5039073	-98.88	34.5096814	153.37	36.4234270	***
32.5128255	-43.95	35.3729502	-159.57	36.4358591	***
33.4014396	251.93	35.3853784	-135.47	36.4482748	220.95
34.3591914	-136.99	35.3978143	***	36.4624989	144.82
34.3752031	-106.86	35.4102357	-147.17	36.4749092	***
34.3881816	-100.98	35.4226507	-207.18	36.4873283	84.96
34.4005943	-115.54	35.4350579	-206.56	36.4997447	198.72
34.4130141	-92.53	35.4547941	-108.45	36.5140711	181.12

Table 5. Radial velocity results for SY Cnc with the Gl 673 template, giving heliocentric julian date (-2447600.0) at mid-exposure and measured heliocentric radial velocity for each of the 42 spectra. The spectra marked with asterisks in the RV column were not used in performing the fit.

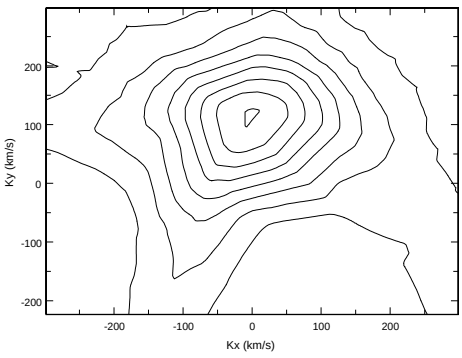

Figure 5. Skew map for SY Cnc, using Gliese 488 (M0−) as the template. Starting from the centre, the contours represent 99%, 85%, 71%, 56%, 42%, 30%, 15% and 1% of the peak height.

The skew map (Fig. 5) has a very clear peak at the expected orbital phase, with no subsidiary noise peaks of comparable size. The skew map satisfied all checks recommended in Vande Putte et al. (2003). These relate to the position of the peak of the skew map and its intensity, to a recognisable sine pattern in the position of the maxima of the cross-correlation functions, and to the resolved features in the average shifted spectrum. This produces the result in Table 6. Fig. 4 displays an orbital average spectrum corrected for this secondary motion and again demonstrates an enhancement of the Na I feature (see Fig. 6 for an expanded view of the region near the Na I doublet). However, the deduced amplitude of the radial velocity curve is considerably less than found from the straightforward cross-correlation study. The errors in that study were re-examined, and it was found that they had been significantly under-estimated, although the value of K_2 was confirmed. The error on K_2 quoted in Table 6 is simply the formal statistical error of the fit; a better estimate of the uncertainty in K_2 from the simple cross-correlation technique is the dispersion about the radial velocity curve. The dispersion is so large that the two results for K_2 are in fact consistent, as can be seen in Table 6, although the value from skew-mapping is believed to be considerably more reliable.

We note that a skew map with the M1.5 template Gl 205 also produces a significant peak, albeit some 15 per cent lower (Vande Putte 2002). With our other templates, the

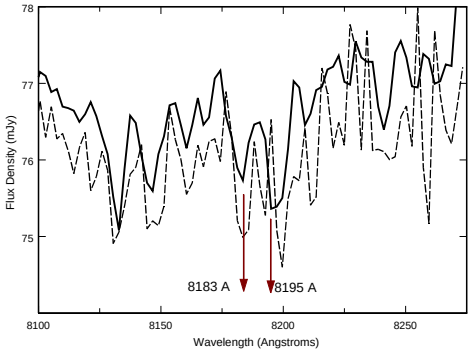

Figure 6. An expanded view of the region of Fig. 4 near 8200 Å, to show the enhancement of the Na I doublet as a result of correcting for the secondary motion. The dashed line shows the average without correction, and the solid line shows the average spectrum after correction; note that the three or four features in the unshifted average combine into just two features, at the correct wavelengths for the Na I doublet.

	Gl 488 M0-	**Gl 673** K7V
RV shift fit:		
γ		-7.2±16
K_2		168.3±15
Dispersion (σ)		68.9±8.9
Skew mapping:		
γ	32±13	
K_2	127±23	
q	0.68±0.14	

Table 6. SY Cnc radial velocity study results ($\mathrm{km\,s^{-1}}$) for the template giving the skew map with the strongest peak (Gl 488), and for the template giving the lowest dispersion radial velocity fit (Gl 673). The results from the simple fit to the radial velocity curve have such a large dispersion that they cannot be used. The last line is the derived mass ratio using Shafter's K_1 value of $86\pm9\,\mathrm{km\,s^{-1}}$.

peak intensities of the maps are much lower, and in some cases the peaks lie at the wrong phase. We are therefore confident that the M0− template provides the best fit amongst our observed templates.

Harrison et al. (2004) have suggested a spectral type of G2 for SY Cnc, based on the relative strengths of absorption lines in infrared spectra over a limited phase range (0.64 to 0.75). We therefore sought a G2 template in the literature, so that we could try a skew map for a wider range of templates. We took two spectra, of spectral types G2V and K0V, from the STELIB compilation of Leborgne et al. (2003), smoothed them to the same resolution as our spectra of SY Cnc, and used them as templates. The resulting skew maps both had much lower intensity peaks than those for our M0− template, and the peaks were at the wrong phases. We are therefore very doubtful that the G2 spectrum found by Harrison et al. represents the average spectrum of the secondary star. We speculate that it may arise from a heated region on the leading hemisphere, which would be preferentially visible in the phase range of their observations. Unfortunately, our data are not of high enough quality to test this by mapping the surface, but other CVs certainly show such regions (e.g. Davey & Smith 1992).

4.2 The unidentified feature

The feature near 8150 Å could not be positively identified. We initially thought that it was an artifact introduced by the extinction correction of the spectra, because the feature appears at roughly the same wavelength as the start of the strong atmospheric water feature which overlies the sodium doublet and which, on these fairly noisy spectra, might have been poorly removed. Certainly, the very strong atmospheric A band was not completely removed – see Fig. 4. However, as indicated in the previous section, masking out the unidentified feature has no effect on the result of skew mapping.

When skew mapping for the individual nights, it was noted that nights 6 and 7 yielded a K_2 and phase within 5% of the original result for all three nights together. Again, masking out the feature had no effect on this. Night 5 on its own, however, does not produce a credible map (the peak line integral is negative). Considering the three nights separately, it appears that the strength of the unidentified feature decreases with time. On night 5, the feature was about twice the strength of the Na I doublet, on night 6 it was about the same strength as the doublet and on night 7 it had decreased to about half the strength of the doublet. From this we surmise that the feature is associated with the outburst, and the decrease in strength may be a sign of the disk gradually becoming optically thin.

4.3 The masses of the components

The most important result in Table 6 is that the mass ratio is now significantly less than unity and is thus completely consistent with the canonical model for mass transfer in CVs. With this independent result for K_2, what can we deduce about the masses of the two stars?

If we first make the common assumption that the secondary just fills its Roche lobe, and lies on the main sequence, we can use Smith & Dhillon's (1998) empirical main sequence mass–period relation to derive the following values of M_1 and M_2 by using our value of q:

$$M_1 = 1.54 \pm 0.40\,\mathrm{M}_\odot$$
$$M_2 = 1.04 \pm 0.11\,\mathrm{M}_\odot\ .$$

The most striking point about this is that the estimate for M_1 is above the maximum mass limit for a white dwarf, although the estimate for M_2 agrees well with that of Shafter (and is consistent with the spectral type of G2 claimed by Harrison et al. 2004). Furthermore, we note that the white dwarf mass is much higher than the average, $(0.84 \pm 0.29)\,\mathrm{M}_\odot$, for Dwarf Novae above the period gap in Smith & Dhillon's (1998) survey. These facts suggest that at least one of the assumptions which led to Shafter's estimate of M_2 is incorrect.

However, given that we now have independent measures of both K_1 and K_2 we can make mass estimates without having to make the assumptions above. The only assumptions we need to make are:

- The stars are in circular keplerian orbits.
- The maximum possible mass for a white dwarf is $\sim$1.44 $\mathrm{M}_\odot$
- We would expect to see some sort of primary eclipse if the inclination were higher than about 71° with this mass ratio (Bailey, 1990).

Horne, Wade and Szkody (1986) describe a Monte Carlo method for inferring the component masses in such an instance. This relies on having reliable values for both K_1 and K_2, and using the mass functions:

$$M_1 \sin^3 i = \frac{PK_2(K_1+K_2)^2}{2\pi G}$$
$$M_2 \sin^3 i = \frac{PK_1(K_1+K_2)^2}{2\pi G}\ .$$

They sample the inclination at random from a uniform distribution over the interval $[0, i_{\max}]$[1]. The values of K_1 and

[1] They found that sampling from a uniform distribution for $\cos i$ rather than i had little effect.

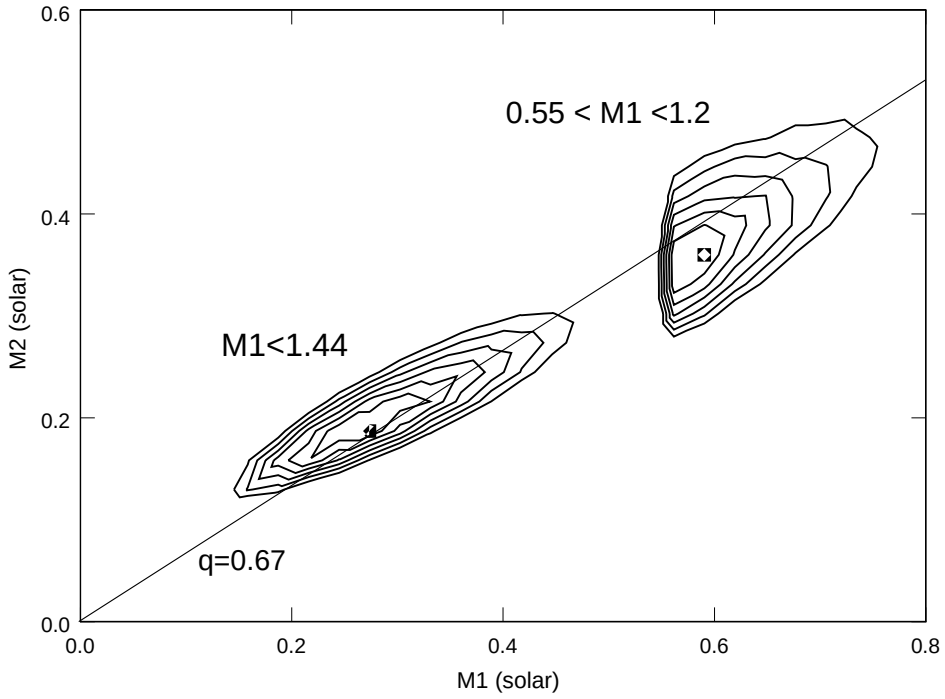

Figure 7. Mass solutions for SY Cancri. The two contour plots represent the frequencies of successful outcomes from a 2×10^7 trial Monte Carlo sampling scheme where i is uniformly distributed over $i = 0 - 71°$, and the primary mass is subject to the two constraints $M_1 \leqslant 1.44\,\mathrm{M}_\odot$ and $0.55 \leqslant M_1/\mathrm{M}_\odot \leqslant 1.22$. The diagonal line labelled $q = 0.67$ represents the stability line for secondary masses less than $0.4342\,\mathrm{M}_\odot$. The lowest contour is at half the maximum frequency. The corresponding plots for a uniform distribution of $\cos i$ are very similar.

K_2 are sampled at random from a normal distribution whose average is the value of the velocity, and standard deviation is the reported error. Using the relations above, M_1 and M_2 are calculated. If M_1 exceeds 1.44 solar masses, the outcome is rejected. The ensuing distribution for accepted outcomes is used to calculate the component masses. A similar calculation was undertaken here, with random sampling from a uniform i over the interval $[0, i_{\max}]$. The results appear in Fig. 7.

From this, we obtain the following values for the system parameters, together with the very similar results (in brackets) from using a uniform distribution of $\cos i$:

$$\begin{aligned} M_1 &= 0.27^{+0.20}_{-0.13}\,\mathrm{M}_\odot & (0.25^{+0.21}_{-0.10}\,\mathrm{M}_\odot) \\ M_2 &= 0.19^{+0.12}_{-0.06}\,\mathrm{M}_\odot & (0.19^{+0.11}_{-0.06}\,\mathrm{M}_\odot) \\ q &= 0.68^{+0.12}_{-0.23} & (0.76^{+0.02}_{-0.35}) \\ i(^\circ) &= 68^{+3}_{-38} & (63^{+8}_{-32}). \end{aligned}$$

If the primary is assumed to be a CO white dwarf with a mass range of $0.55M_\odot$ to $1.22M_\odot$, then these values become:

$$\begin{aligned} M_1 &= 0.59^{+0.16}_{-0.04}\,\mathrm{M}_\odot & (0.56^{+0.15}_{-0.02}\,\mathrm{M}_\odot) \\ M_2 &= 0.36^{+0.14}_{-0.08}\,\mathrm{M}_\odot & (0.33^{+0.13}_{-0.06}\,\mathrm{M}_\odot) \\ q &= 0.61^{+0.02}_{-0.21} & (0.59^{+0.10}_{-0.20}) \\ i(^\circ) &= 52 \pm 19 & (55^{+16}_{-20}). \end{aligned}$$

These results are also plotted in Fig. 7. Each value corresponds to the peak of the relevant distribution. Note that the value of i is significantly larger than estimated by Shafter (1983).

The two sets of parameters are distinct, so we need some way of choosing between them. It turns out that they are in a mass ratio range that is close to the condition for dynamical instability for mass transfer. According to Politano (1996), for $M_2 \leqslant 0.4342\,\mathrm{M}_\odot$ mass transfer occurs on a dynamical timescale for $q \geqslant 0.67$. Our first set of parameters therefore correspond formally to unstable mass transfer (especially for the uniform $\cos i$ case), although the errors are large enough to make a firm conclusion impossible. However, the second set of parameters appears to be more definitely below the stability line, except possibly for the uniform $\cos i$ case. We therefore prefer the second set of parameters and will adopt them in the later discussion.

5 FLUX VARIATIONS AROUND THE ORBIT

5.1 I-band photometry

Because of the relatively long orbital period, none of the three nights of photometric data covers a complete range of phase and it is necessary to combine the three nights in order to discover how the I-band flux varies around the orbit. If the system were in quiescence, this would be relatively

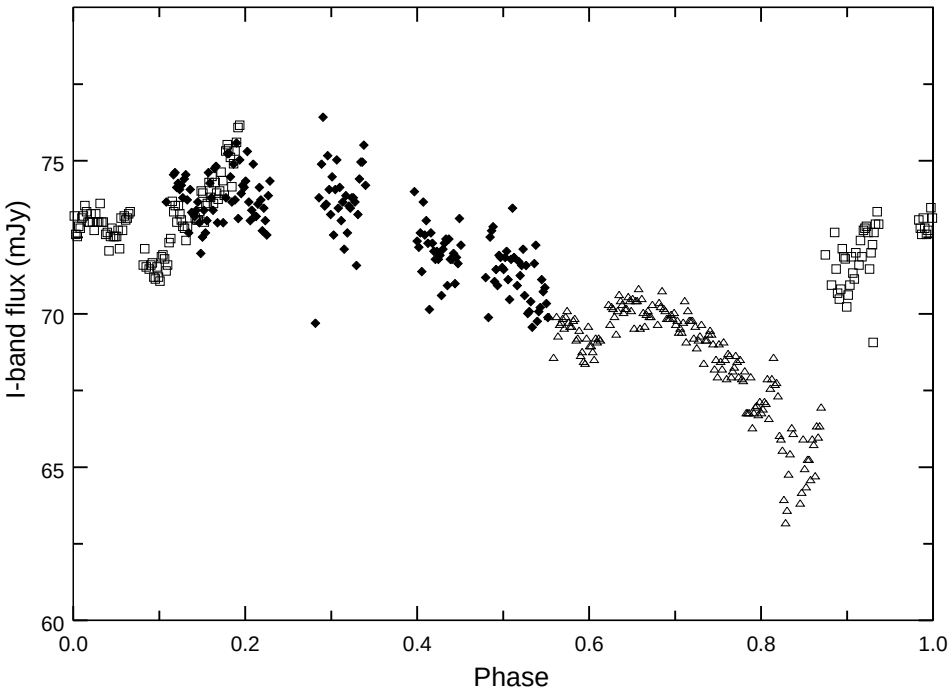

Figure 8. The variation around the orbit of the I-band flux, adjusted to the flux scale of night 7. Different nights are indicated by different filled symbols: square – night 5; triangle – night 6; diamond – night 7. Phase zero corresponds to the inferior conjunction of the red dwarf.

straightforward. Because it is in decline from outburst, it is necessary to devise some way of taking out the night-to-night variations before the orbital variations are sought.

Inspection of Fig. 1 and Table 4 shows that the decrease in brightness is less than 0.1 mag from one night to the next. The typical duration of the observing run on a single night was less than 4 hours, so the general decrease in brightness during a night's observation was less than 0.017 mag, smaller than the typical uncertainty of 0.03 mag in an individual point. We therefore initially took out the night-to-night variations simply by computing the average magnitude for each night and subtracting the appropriate night's average magnitude from each observed point. We then plotted the magnitude differences as a function of orbital phase, and it became apparent that the three nights had very little overlap in phase and that there was considerable variation around the orbit. This meant that even in quiescence we would not expect the average magnitude to be the same for each night, as we had tacitly assumed.

Although the three nights cover almost disjoint ranges of phase, there is a very slight overlap, especially between nights 5 and 7. We therefore adopted a different strategy. We first converted the magnitudes to fluxes, and then adjusted the mean flux for the data on nights 5 and 6 in such a way that the fluxes in the overlapping ranges of phase matched. Because there is considerable scatter in the flux curve, and the phase overlap is very small, this procedure is not very precise. However, it produces a plausible looking light curve, which is presented in Fig. 8. The total range of the variation is about 0.2 mag, or about 20 per cent in flux. Because the simultaneous spectroscopic data cover a slightly larger phase range, they were used to confirm that the flux adjustment had been done consistently. We fitted a 3rd-order polynomial to the continuum of each spectrum, between 7875 Å and 8075 Å to avoid the strongest lines, and used these polynomial fits to produce an indicative continuum flux for each spectrum. We then adjusted the mean flux for these data on nights 5 and 6 so that the fluxes in the somewhat larger overlapping phase ranges matched; the resulting continuum light curve is broadly similar to the I-band light curve, and in particular confirms the fitting between the different nights. However, there is no large line-free region of continuum to which to do the fitting, so the continuum light curve is not a very reliable indicator of the more detailed flux variations around the orbit and we do not present it here.

The main feature of the I-band curve is the drop to a relatively deep minimum at about phase 0.85, and an apparently rapid recovery from it. This looks almost like an eclipse, but the phase is wrong, the curve is rather asymmetric and the inclination of the system is too low. The light curve also displays a surprisingly large scatter about the mean curve, especially on nights 7 (diamonds) and 6 (triangles). Because we only just cover the entire phase range, it is not clear whether either of these features would repeat from one cycle to the next. The somewhat different behaviour in the phase range 0.1 to 0.2 on nights 5 and 7 suggests that they do not, and that we may simply be seeing fluctuations in the disc brightness as it adjusts its structure after the

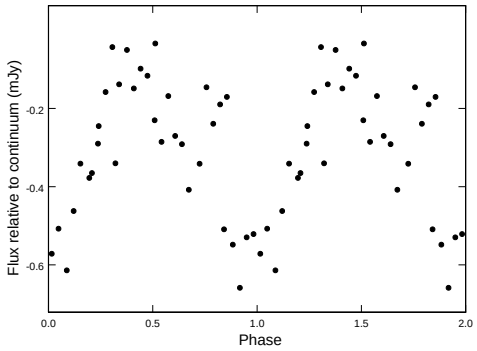

Figure 9. The integrated flux (mJy) in the OI absorption triplet as a function of orbital phase.

outburst. Even the minimum at phase 0.85 may arise from such fluctuations, and we refrain from speculating on its significance until a better light curve is available.

5.2 Spectroscopic variations: the OI line

The OI triplet absorption feature at 7773Å is generally believed to arise in the accretion flow, and is usually strong in nova-like systems (e.g. V1315 Aql; Smith et al. 1993b). However, it is also reasonably prominent in this dwarf nova (Fig. 2), presumably because the disc is still in a bright post-outburst state, and we may use it to probe the nature of the accretion flow.

We therefore measured the equivalent width of the absorption feature as a function of orbital phase. Because some of the individual spectra are rather noisy, the measurements were made several times and the results averaged. In addition, we also measured the flux deficit for the feature by fitting the entire continuum by a low order cubic spline function, using that to normalise the spectrum, subtracting 1 from the resulting spectrum and integrating over the (negative) absorption feature. All the results were consistent. The flux deficit curve is shown in Fig. 9, plotting two orbital cycles for clarity.

The curve appears to be roughly sinusoidal, with a maximum absorption strength around phase 0.9–1.0 and a broad minimum around phase 0.4. There also appears to be a poorly defined but strong dip in absorption line strength around phase 0.8; it is present in both the flux and equivalent width plots, so it is probably real. However, it is not what is expected from a symmetrical disc. Since it is only defined by four points, we do not try to interpret it.

If the absorption feature arose in the bright spot, it would be expected to be at maximum strength when the observer was looking most directly at the bright spot, which would be around phase 0.9. Because the absorption feature is strong, we tried to verify this interpretation by measuring its radial velocity curve. The template used for cross-correlation was formed by taking one of the spectra in which the OI line was strongest and replacing the spectrum outside the line by a smooth fit to the continuum, which was then normalised to unity. However, the radial velocity curve obtained from standard cross-correlation analysis was too noisy for any conclusions to be drawn.

We then attempted a skew-mapping approach, as described above for the Na I feature. This produced the interesting result that the OI feature appears to be formed very close to the centre of mass of the system: the skew map is consistent with the peak being exactly at the centre of mass, but the peak is broad enough to be consistent also with a position rather closer to the bright spot; formally, $K_{\rm x} = +1 \pm 42\,{\rm km\,s^{-1}}$, $K_{\rm y} = -8 \pm 19\,{\rm km\,s^{-1}}$. When interpreted as a radial velocity curve, the amplitude is $8 \pm 26\,{\rm km\,s^{-1}}$ and the zero-crossing from positive to negative velocities is at phase $0.98^{+0.24}_{-0.20}$, which is consistent with its tracking the motion of the bright spot.

We therefore conclude that the OI feature comes primarily from the bright spot.

6 CONCLUSIONS

Our measurement of the secondary star radial velocity curve for SY Cancri leads us to conclude that the mass ratio in this system is indeed *less* than unity, as is the case for most CVs. This result disagrees with the work of Shafter (1983), and must mean that one or more of his assumptions is incorrect for SY Cnc. Despite the fact that it is now clear that *on average* the secondary stars of CVs cannot be distinguished from main-sequence stars (Warner 1995, Sections 2.8 & 2.9; Smith & Dhillon 1998), the most likely assumption to be wrong *for an individual star* is the use of a main sequence mass-radius relation. Our results show that, with the long period of the system and the observed mass ratio, the secondary star cannot be on the main sequence unless the primary is a neutron star rather than a white dwarf (or at least is an unusually massive white dwarf). If it were a neutron star, we would expect the system's behaviour to be quite different from that observed. A very massive white dwarf might just be accommodated. However, a main sequence Roche-lobe filling star would have a mass of $1.04\,{\rm M}_\odot$, which would correspond to a spectral type of about G2, very different from the M0– suggested by the skew mapping (see Section 4.1).

Our conclusion therefore is that the secondary star in SY Cancri is substantially lighter than a main-sequence star of the same size (or alternatively much larger than a main-sequence star of the same mass). From values in Allen (1973, p.209) we find that a main-sequence M0 star should have a mass of approximately $0.47\,{\rm M}_\odot$; the same mass was quoted by Martin (1988, Table B1) for a spectral type M0.5±1. This is just about consistent within the errors with our preferred value of $0.36^{+0.14}_{-0.08}\,{\rm M}_\odot$, which would correspond to a spectral type of about M2.5 according to Martin's Table B1. However, a main-sequence star of that mass would have a radius considerably less than the Roche lobe radius. The star does fill its Roche lobe and must therefore be much larger than its main-sequence radius. Normally, this would imply a star that was also much cooler than the spectral type corresponding to its mass, but this star is if anything slightly hotter than expected.

We therefore seem to have a star that is both considerably larger than a main-sequence star of its mass, and also slightly hotter (at M0) than the spectral type (M2.5) expected from its mass. It must therefore be considerably

more luminous than a main-sequence star of $0.36\,M_\odot$. At a period of over 9 hours, the secondary may well be slightly evolved, which could account both for the larger radius and the larger luminosity, although the low present-day mass suggests that the evolution took place long ago and that the system is very old. The radius is also expected to be somewhat enlarged compared to the main-sequence value by the star being out of thermal equilibrium. Irradiation of the secondary by the primary/disc may also cause some expansion.

Irradiation can show up as a distortion of the radial velocity curve (e.g. Davey & Smith 1992). There seems to be no sign of that, since the RV curve is not significantly elliptical. However, the RV curve is also very noisy, and Catalán, Schwope & Smith (1999) show that if the irradiation is symmetrical about the line of centres there may be significant heating without there being a significant eccentricity in the orbital solution. If irradiation is important, the value of K_2 will need some correction. However, with a relatively long period, and correspondingly relatively large separation, the irradiation is very unlikely to affect the value of K_2 by enough to change our main conclusions that the secondary star in SY Cnc is substantially less massive than found by Shafter (1983) and departs markedly from a main-sequence mass-radius relationship.

Acknowledgments

Nigel Hawkins was supported by a SERC studentship. The data reduction and analysis were carried out at the Sussex node of the PPARC Starlink Project. The Jacobus Kapteyn and Isaac Newton Telescopes were operated by the Royal Greenwich Observatory at the Observatorio del Roque de los Muchachos of the Instituto de Astrofísica de Canarias. We are grateful to Drs Vik Dhillon and Derek Jones for assistance with the observing.

REFERENCES

Allen, C. W., 1973, Astrophysical Quantities, 3rd edition, Athlone Press, London
Argyle, R. W., Mayer, C. J., Pike, C. D., Jorden, P. R., 1988, User Manual No. 18: A User Guide to the JKT CCD Camera, Isaac Newton Group, La Palma
Bailey, J. A., 1990, MNRAS, 243, 57
Bassett, E. E., 1978, Observatory, 98, 122
Bessell, M. S., 1979, PASP, 91, 589
Catalán, M. S., Schwope, A. D., Smith, R. C., 1999, MNRAS, 310, 123
Davey, S. C., Smith, R. C., 1992, MNRAS, 257, 476
Dhillon, V. S., 1990, Ph.D. thesis, University of Sussex, UK
Friend, M. T., Martin, J. S., Smith, R. C., Jones, D. H. P., 1988, MNRAS, 233, 451
Friend, M. T., Martin, J. S., Smith, R. C., Jones, D. H. P., 1990a, MNRAS, 246, 637
Friend, M. T., Martin, J. S., Smith, R. C., Jones, D. H. P., 1990b, MNRAS, 246, 654
Harrison, T. E., Osborne, H. L., Howell, S. B., 2004, AJ, 127, 3493
Horne, K., 1986, PASP, 98, 609
Horne, K., Wade, R.A., Szkody, P, 1986, MNRAS, 219, 791
King, A. R., 1988, QJRAS, 29, 1
King, D. L., 1988, Technical Note No. 31, RGO
Leborgne, J.-F., Bruzual, G., Pello, R., Lançon, A., Rocca-Volmerange, B., Sanahuja, B., Schaerer, D., and two others, 2003, A&A, 402, 433
Martin, J. S., 1988, Ph.D. thesis, University of Sussex
Oke, J. B., 1990, AJ, 99, 1621
Oke, J. B., Gunn, J. E., 1983, ApJ, 266, 713
Patterson, J., 1981, ApJS, 45, 517
Politano, M., 1996, ApJ, 465, 338
Ritter, H., Kolb, U., 2003, A&A, 404, 301
Shafter, A. W., 1983, Ph.D. thesis, University of California, Los Angeles, U.S.A.
Smith, D. A., Dhillon, V.S., 1998, MNRAS, 301, 767
Smith, R. C., Collier Cameron, A., Tucknott, D. S., 1993a, in Regev, O., Shaviv, G., eds, Cataclysmic Variables and Related Physics, Proceedings of the 2nd Technion Haifa Conference, Institute of Physics Publishing and The Israel Physical Society, in association with The American Institute of Physics, p. 70
Smith, R. C., Fiddik, R. J., Hawkins, N. A., Catalán, M. S., 1993b, MNRAS, 264, 619
Smith, R. C., Hawkins, N. A., Mehes, O., 2000, in Charles, P. A., King, A., O'Donoghue, D., eds, Proceedings of the Symposium in Honour of Professor Brian Warner, Oxford, April 1999, *New Astronomy Reviews*, 44, p. P31
Szkody, P., 1981, ApJ, 247, 577
Tonry, J., Davis, M., 1979, AJ, 84, 1511
Turnshek, D. E., Turnshek, D. A., Craine, E. R., Boeshaar, P. C., 1985, An Atlas of Digital Spectra of Cool Stars, Western Research Company, Tucson, Arizona, USA
Vande Putte, D., 2002, Master's thesis, University of Sussex, UK
Vande Putte, D., Smith, R.C., Hawkins, N.A., Martin, J.S., 2003, MNRAS, 342, 151
Warner, B., 1995, Cataclysmic Variable Stars, Cambridge University Press, Cambridge

This paper has been typeset from a TEX/ LATEX file prepared by the author.